

The very steep spectrum radio halo in Abell 697

G. Macario^{1,2}, T. Venturi¹, G. Brunetti¹, D. Dallacasa^{1,2}, S. Giacintucci^{3,1}, R. Cassano¹, S. Bardelli⁴, and R. Athreya⁵

¹ INAF – Istituto di Radioastronomia, via Gobetti 101, I-40129, Bologna, Italy

² Dipartimento di Astronomia, Università di Bologna, via Ranzani 1, I-40127, Bologna, Italy

³ Harvard–Smithsonian Centre for Astrophysics, 60 Garden Street, Cambridge, MA 02138, USA

⁴ INAF–Osservatorio Astronomico di Bologna, via Ranzani 1, I-40127, Bologna, Italy

⁵ Indian Institute of Science Education and Research, Sutarwadi Road, Pashan, Pune 411021, INDIA

Received 00 - 00 - 0000; accepted 00 - 00 - 0000

ABSTRACT

Aims. In this paper we present a detailed study of the giant radio halo in the galaxy cluster Abell 697, with the aim to constrain its origin and connection with the cluster dynamics.

Methods. We performed high sensitivity GMRT observations at 325 MHz, which showed that the radio halo is much brighter and larger at this frequency, compared to previous 610 MHz observations. In order to derive the integrated spectrum in the frequency range 325 MHz–1.4 GHz, we re-analysed archival VLA data at 1.4 GHz and made use of proprietary GMRT data at 610 MHz.

Results. Our multifrequency analysis shows that the total radio spectrum of the giant radio halo in A 697 is very steep, with $\alpha_{\frac{1.4\text{GHz}}{325\text{MHz}}} \approx 1.7 - 1.8$. Due to energy arguments, a hadronic origin of the halo is disfavoured by such steep spectrum. Very steep spectrum halos in merging clusters are predicted in the case that the emitting electrons are accelerated by turbulence, observations with the upcoming low frequency arrays will be able to test these expectations.

Key words. radiation mechanism: non-thermal – galaxies: clusters: general – galaxies: clusters: individual: A 697

1. Introduction

Radio halos are diffuse low surface brightness radio sources extended on Mpc scales, observed in the central regions of a fraction of X-ray luminous (i.e. massive) galaxy clusters. Their synchrotron emission is not associated with individual galaxies, but it originates from the non-thermal component of the intracluster medium (ICM). They provide the most important piece of evidence for the presence of relativistic (\sim GeV) electrons and μ G magnetic fields in galaxy clusters (see Ferrari et al. 2008 for a recent review). To date radio halos have been found from large sky surveys (such as the Northern VLA Sky Survey, NVSS, Condon et al. 1998 and the Westerbork Northern Sky Survey, WENSS, Rengelink et al. 1997; i.e. Giovannini et al. 1999; Kempner & Sarazin 2001), and from pointed observations of individual clusters, mostly carried out at 1.4 GHz (Govoni et al. 2001; Bacchi et al. 2003; and the recent compilation by Giovannini et al. 2009) and at 610 MHz (the GMRT Radio Halo survey, Venturi et al. 2007 and 2008, hereinafter VGB07 and VGD08). They have steep radio spectra, with $\alpha \sim 1.2 - 1.4$ ($S \propto \nu^{-\alpha}$) from integrated flux density measurements.

The origin of radio halos is a long-standing problem, since the radiative life-time of the relativistic electrons responsible for their synchrotron emission is much shorter than the particle diffusion time required to cover their Mpc extent (Jaffe 1977). This requires some form of particle re-acceleration. So far two main models have been proposed to explain the origin of radio halos: (1) the “re-acceleration model”, whereby radio halos originate from the in-situ re-acceleration of pre-existing electrons by magneto-hydrodynamic (MHD) turbulence injected in the ICM during cluster mergers (Brunetti et al. 2001; Petrosian 2001; Brunetti & Blasi 2005); (2) “secondary electron models”, predicting that relativistic electrons are injected in the cluster

volume by hadronic collisions between relativistic cosmic rays and the thermal protons of the ICM (e.g. Dennison 1980; Blasi & Colafrancesco 1999).

Recent radio observations provide indirect evidence for turbulent acceleration in the ICM (e.g. Brunetti et al. 2008). Observational support to the “re-acceleration scenario” is also given by the growing evidence for the connection between cluster mergers and radio halos, based on high sensitivity radio and X-ray observations (Buote 2001; Govoni et al. 2004; VGD08 and references therein; Giacintucci et al. 2009; Cassano 2009), and by constraints to the evolution of radio halos (Brunetti et al. 2009).

The analysis of the radio spectrum of halos is important to address the question of their origin. The turbulent re-acceleration model provides the unique expectation of spectra much steeper than those found to date, as a consequence of less energetic merger events (e.g. Cassano 2009). The detection of radio halos with very steep spectrum ($\alpha > 1.6$) would be a major piece of evidence in support of this scenario, and at the same time it would disfavour a secondary origin of the electrons, which requires a very large proton energy budget (e.g. Brunetti 2004). The prototype of these sources, which we refer to as *ultra steep spectrum radio halos* (hereinafter USSRH), has been recently discovered in the merging cluster A 521 and has a spectrum with $\alpha \sim 1.9$ (Brunetti et al. 2008; Dallacasa et al. 2009). In this paper we present a detailed study of the merging cluster A 697, which hosts a candidate steep spectrum radio halo. Our work is based on proprietary GMRT radio observations at 610 and 325 MHz, and data from the VLA public archive at 1.4 GHz.

A 697 is a rich and massive galaxy cluster located at $z=0.282$, belonging to the Abell, Corwin and Olowin catalogue (ACO catalogue, Abell et al. 1989). The cluster is hot and luminous in the X-ray band, and is part of the ROSAT Brightest

Table 1. General properties of the galaxy cluster A 697.

RA _{J2000}	08h 42m 53.3s
DEC _{J2000}	+36° 20′ 12″
Bautz–Morgan Class	II–III
Richness	1
z	0.282
σ_v	1334 km s ⁻¹ (a)
L _{X[0.1–2.4keV]}	10.57 × 10 ⁴⁴ erg s ⁻¹
M _V	2.25 × 10 ¹⁵ M _⊙ (b)
R _V	2.90 Mpc (b)

Notes to Table 1: (a): Girardi et al. 2006; (b): Estimated from the L_X–M_V relation, see Eq. 6 and 7 in Cassano et al. (2006).

Cluster Sample (BCS; Ebeling et al. 1998). Its general properties are summarized in Table 1¹, which provides: coordinates; morphological classification of the cluster and richness; redshift z; cluster velocity dispersion σ_v (from optical spectroscopy); X-ray luminosity L_X (taken from the BCS catalogue); virial mass M_V and the corresponding virial radius R_V. The presence of diffuse cluster-scale radio emission in A 697 was first suggested in Kempner & Sarazin (2001) by inspection of the NVSS and the WENSS, and further confirmed by observations at 610 MHz with the Giant Metrewave Radio Telescope (GMRT) as part of the GMRT Radio Halo Survey (VGB07 and VGD08). From those observations the extended radio emission at the cluster centre has been unambiguously classified as a giant² radio halo.

The paper is organized as follows. In Sect. 2 we present the new 325 MHz GMRT data; in Sect. 3 and 4 we derive the integrated spectrum and discuss the sources of uncertainty in the flux density measurements; in Sect. 5 we discuss the origin of the A 697 radio halo in the framework of the turbulent re-acceleration model. Summary and conclusions are given in 6.

2. GMRT radio data at 325 MHz

2.1. Radio observations and data reduction

The main characteristics of the 325 MHz observations are summarised in Table 2, which reports: observing date, frequency, total bandwidth, total time on source, synthesized half power beamwidth (HPBW), rms level (1 σ) at full resolution and u–v range of the full dataset.

The observations were carried out using simultaneously the upper and lower side bands (USB and LSB, respectively), for a total observing bandwidth of 32 MHz. The default spectral-line observing mode was performed, with 128 channels for each band and a spectral resolution of 125 kHz/channel. The USB and LSB datasets were calibrated and analyzed separately using the NRAO Astronomical Image Processing System package (AIPS). 3C 147 and 3C 286 were used as primary calibrators, and were observed respectively at the beginning and at the end of the observing run. The point source 0735+331 was used as phase calibrator.

Due to the considerably lower quality of the LSB (strong RFI residuals), only the USB data were used to produce the final im-

ages presented and analysed in this paper.

The very large field of view of the GMRT at 325 MHz (primary beam $\sim 1.8^\circ$) required the implementation of the wide-field imaging technique in each step of the self-calibration process, in order to account for the non-planar nature of the sky. We covered a field of view as large as $\sim 2.7 \times 2.7$ square degrees with 25 facets, to include possible strong sources located beyond the primary lobe, conventionally cut at 5%. We initially self-calibrated the longest baselines using only the point sources in the field, then we progressively included short baselines and resolved radio sources. Finally we included also the emission from the radio halo. Note that only phase self-calibration was applied.

Even though only half of the full dataset was usable, the quality of the final image is very good: the rms ranges from $\sim 45 \mu\text{Jy b}^{-1}$ to $\sim 55 \mu\text{Jy b}^{-1}$. Despite the relatively low frequency, confusion in this image is negligible, due to the arcsecond resolution. The residual amplitude errors on each individual antenna are $\leq 5\%$. On the basis of this result we can conservatively assume that the absolute flux density calibration is within 5%. Such value accounts for the uncertainty in the calibrator flux density scale as well.

2.2. The field

In Fig. 1 we report the 325 MHz GMRT full resolution contours of the central $12' \times 12'$ ($\sim 3 \times 3 \text{ Mpc}^2$) portion of the A 697 field. The region corresponds to half the cluster virial radius ($R_V = 2.9 \text{ Mpc}$, Table 1). The most prominent features at this resolution are the two extended radio galaxies, labelled as S1 and S2 in Fig. 1, located South of the cluster centre. In addition, the diffuse radio emission associated with the radio halo is clearly visible around the cluster centre.

2.3. The radio halo

Fig. 2 zooms into the central cluster region. The left panel shows the full resolution 325 MHz contours (starting from $\pm 3\sigma$), overlaid on the red optical frame from the Digitized Palomar Sky Survey (DSS–2). Beyond the individual radio sources with optical counterpart, diffuse emission is clearly visible at the cluster centre. Three discrete radio sources embedded in the halo emission are optically identified with cluster members (Girardi et al. 2006, hereinafter G06). We labelled them A, D and G, following the same notation used for the corresponding sources identified in the GMRT 610 MHz full resolution image (left panel of Fig. 2, see also VGD08). In Table 3 we report their radio position and flux density at 325 MHz (obtained from Gaussian fits in the full resolution image), together with their optical identification and redshift (from G06). Source A is identified with the central cD galaxy.

In order to properly image the diffuse emission of the radio halo, the three sources A, D and G, whose total flux density amounts to $S_{325 \text{ MHz}} = 7.96 \text{ mJy}$, were subtracted from the u–v data. The final “subtracted” dataset was used to produce images of the radio halo at various angular resolutions, tapering the u–v data by means of the parameters robust and uvtaper in the task IMAGR.

In the right panel of Fig. 2 we report the 325 MHz contours of the radio halo at the resolution of $46.8'' \times 41.4''$, overlaid on a GMRT 610 MHz image of similar resolution and obtained with a comparable weighting scheme ($46.4'' \times 35.9''$; grey scale, see also VGD08). The first contour corresponds to the $\pm 3\sigma$ signifi-

¹ We adopt the Λ CDM cosmology with $H_0 = 70 \text{ km s}^{-1} \text{ Mpc}^{-1}$, $\Omega_m = 0.3$ and $\Omega_\Lambda = 0.7$. At the redshift of A 697 ($z = 0.282$), this cosmology leads to a linear scale of $1'' = 4.26 \text{ kpc}$.

² Linear size $\gtrsim 1 \text{ Mpc } h_{50}^{-1}$.

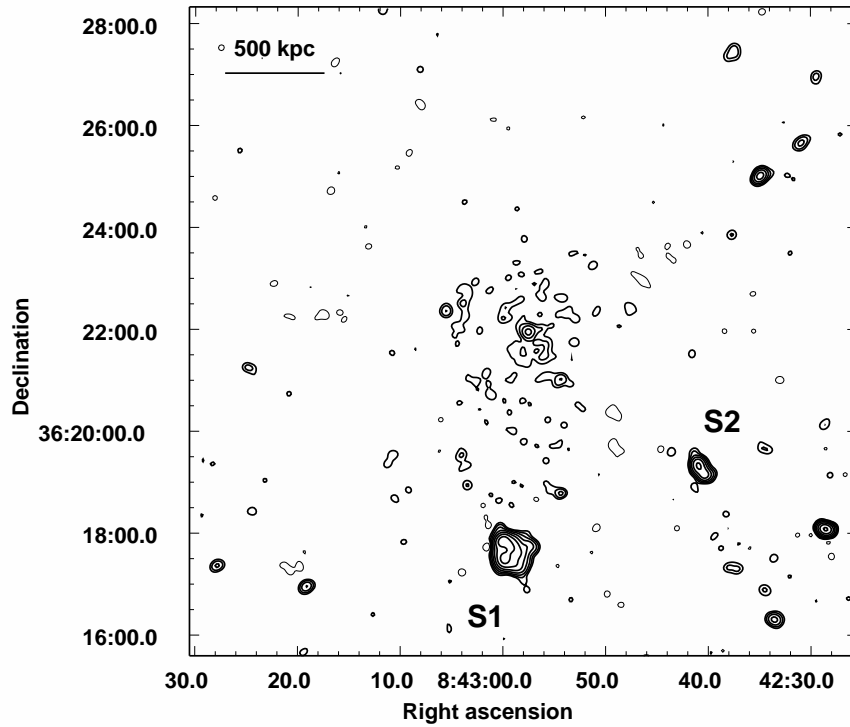


Fig. 1. GMRT 325 MHz radio contours of the inner $12' \times 12'$ region centered on A 697. The 1σ level in the image is $45 \mu\text{Jy b}^{-1}$. Contours are spaced by a factor 2 starting from $5\sigma = \pm 0.225 \text{ mJy b}^{-1}$. The HPWB is $10.0'' \times 9.1''$, p.a. -64° . The labels S1 and S2 indicate the two extended radio galaxies in the Southern part of the cluster.

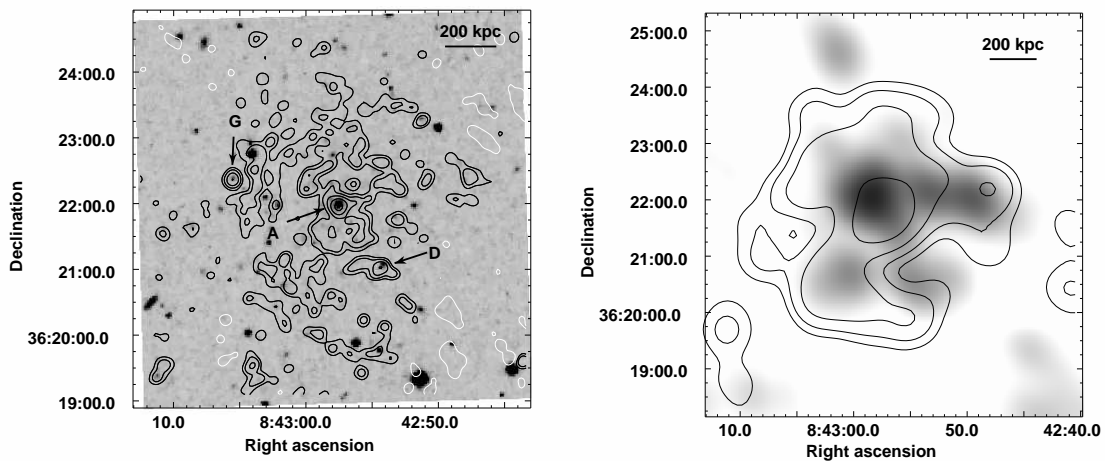


Fig. 2. *Left* – Full resolution GMRT 325 MHz contours of the central region of A 697, superposed to the Second Palomar Sky Survey (POSS-2) optical image. The image is the same as Fig. 1 ($10.0'' \times 9.1''$, p.a. -64° , 1σ level is 0.045 mJy b^{-1}) and contours are spaced by a factor of 2, starting from $\pm 0.135 \text{ mJy b}^{-1}$ (3σ). Individual radio sources are labelled by letters A, D and G (as in VGD08, Fig. 2). *Right* – Low resolution GMRT image at 325 MHz of the radio halo (obtained after subtraction of the individual sources, see Sect. 2.3) overlaid on the GMRT 610 MHz image (grey scale). The resolution of the 325 MHz image is $46.8'' \times 41.4''$, p.a. 80° , and the 1σ noise level is 0.15 mJy b^{-1} . Logarithmic contours are shown, starting from $\pm 0.45 \text{ mJy b}^{-1}$. The 610 MHz image has a resolution of $46.4'' \times 35.9''$, p.a. 42° , and the 1σ noise level is 0.05 mJy b^{-1} .

Table 2. Summary of the GMRT radio observations.

Observation date	ν (MHz)	$\Delta\nu$ (MHz)	t (min)	HPBW, p.a. (full array, "x", °)	rms ($\mu\text{Jy b}^{-1}$)	$u-v$ range ($k\lambda$)
17 Jan 2007	325	32(16)*	480	10.0x9.1, -64	45	~0.08-25

Notes to Table 2: * The observations were performed using a total bandwidth of 32 MHz (USB+LSB), but only the USB dataset was used for the analysis (see Sect. 2.1)

Table 3. Individual radio galaxies at the center of A 697.

Radio source	Radio position RA _{J2000} & DEC _{J2000}	S _{325 MHz} mJy	Optical Position RA _{J2000} & DEC _{J2000}	z
A	08 42 57.70 +36 22 01	4.63±0.23	08 42 57.55 +36 22 00	0.281
D	08 42 54.54 +36 21 05	1.97±0.10	08 42 54.36 +36 21 03	0.274
G	08 43 05.65 +36 22 25	1.36±0.07	08 43 05.50 +36 22 24	0.267

cance level.

The radio halo of A 697 is very extended at 325 MHz, with a largest angular size (LAS) of $\sim 5.1'$, corresponding to a largest linear size (LLS) of $\sim 1.3 \text{ Mpc } h_{70}^{-1}$. Its overall morphology is regular and symmetric, and more extended than imaged at 610 MHz. The central $\sim 1'$ is similar at both frequencies, and the bright feature well visible at 610 MHz in the western part of the halo is almost coincident with a similar structure at 325 MHz.

The total integration time of the 610 MHz observations is much shorter than that at 325 MHz (see section 2.1), and the $u-v$ coverage of the short spacings worse. In Fig. 3 we report a comparison between the inner portions of the $u-v$ plane at 325 and 610 MHz (left and right panel respectively); visibilities relative to baselines shorter than $1 k\lambda$ are shown³. For this reason, a detailed spectral index imaging was not carried out.

The total flux density of the radio halo at 325 MHz is $S_{325\text{MHz}} = 47.3 \text{ mJy}$ (see Sect. 4 for a detailed discussion on the uncertainties associated with this value); it was obtained by integrating the low resolution image (Fig. 2, right panel) over the region covered by the $\sim 3\sigma$ contour. The corresponding total radio power is $\log P_{325 \text{ MHz}} (\text{W/Hz}) = 25.07$.

3. The integrated radio spectrum of the halo

In order to derive the spectrum of the giant radio halo in A 697 with at least three data points, we complemented the GMRT flux density values at 610 MHz and 325 MHz with archival 1.4 GHz VLA-C public data.

3.1. VLA archive data at 1.4 GHz

We re-analyzed archival VLA-C observations at 1.4 GHz (Obs. Id. AJ0252). These are short observations centered on A 697, with total integration time of ~ 50 minutes and $u-v$ range $0.3-15 k\lambda$. After the usual a-priori calibration, the final images were obtained after a few iterations of phase-only self-calibration.

We successfully detected diffuse emission at the cluster centre. In order to account for the contribution of the point sources in the halo region, we produced an image using only baselines longer than $3 k\lambda$, to rule out the contribution of the halo emission (resolution $\sim 9'' \times 11''$). The 1σ rms is $\sim 12 \mu\text{Jy b}^{-1}$. In the central

halo region we identified 7 point sources, with peak flux density exceeding 5 times the rms level; two of them were already found at 610 MHz, and labelled A (the central cD) and F in VGD08. We fitted all sources with individual Gaussians, and obtained a total contribution to the integrated flux density of $S_{1.4 \text{ GHz}} = 0.97 \text{ mJy}$. In Fig. 4 we show a low resolution image of the radio halo at 1.4 GHz (restoring beam of $35'' \times 35''$) for comparison with the 325 MHz and 610 MHz images. The crosses mark the position of the embedded radio point sources. Note that the field shown is the same as the right panel of Fig. 2.

At 1.4 GHz the radio halo appears considerably smaller than in the GMRT images. It is elongated in the East-West direction, in agreement with the brightest part of the 610 MHz emission. The LAS is $\simeq 190''$, corresponding to a LLS $\simeq 810 \text{ kpc } h_{70}^{-1}$. Its total flux density is $S_{1.4 \text{ GHz}} = 3.7 \text{ mJy}$, corresponding to a radio power $\log P_{1.4 \text{ GHz}} (\text{W/Hz}) = 23.95$. This value was obtained by integrating this image over the same area covered by the radio halo at 325 MHz, and after subtraction of the total contribution of the embedded point sources.

Hints of diffuse emission at the centre of A 697 are visible on the NVSS 1.4 GHz image (Fig. 5, left panel). However, after an accurate inspection we concluded that this image is affected by fringe residuals (see Giacintucci 2007). For this reason, the NVSS pointing containing the A 697 field was imaged after a new calibration. We found out that one IF was affected by strong interference, and it was necessary to remove it from the self-calibration and imaging process. The new image is reported in the central panel of Fig. 5: indeed, no extended emission is detected at the cluster centre at the noise level of $\sim 0.3 \text{ mJy b}^{-1}$. Our re-analysis confirmed that the extended structure visible in the public NVSS image is coincident with a peak of a residual fringe, which crosses the image along the NW-SE direction, i.e. the same direction of the structure itself. Some residual patterns are still visible in the recalibrated image at the 1σ level. The right panel of Fig. 5 reports the recalibrated NVSS image (contours) overlaid on the 1.4 GHz VLA-C image (grey scale). The non-detection on the recalibrated NVSS image is consistent with the VLA-C image, given the rms, peak and restoring beams in the two images (see figure caption). We integrated the flux density on the recalibrated NVSS image over the same sky portion covered by the radio halo at 1.4 GHz, and measured 2.4 mJy . Considering that the contribution of point sources in this region

³ The angular size of the halo ($\sim 5'$) is sampled by visibilities corresponding to baselines shorter than $\sim 0.7 k\lambda$.

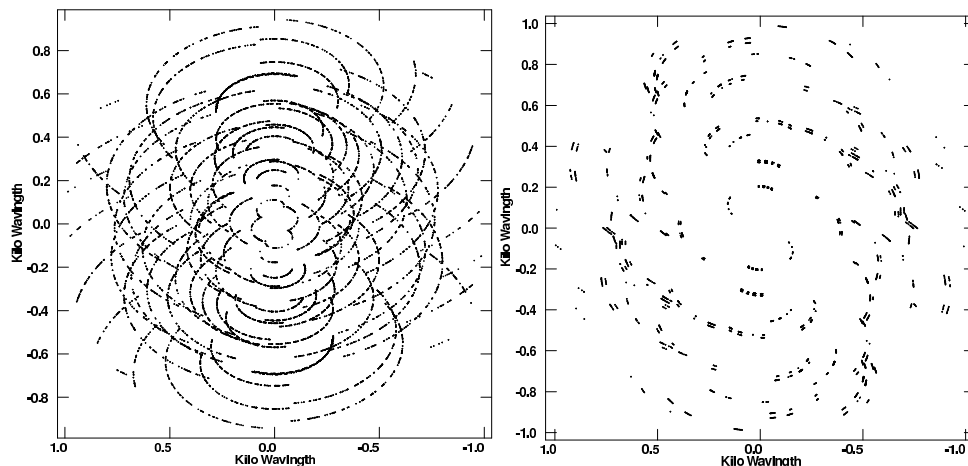


Fig. 3. Comparison between the inner portion of the u - v plane sampled by the GMRT observations at 325 MHz (*left panel*) and at 610 MHz (*right*) from which the flux density measurements of the halo has been taken. Only baselines shorter than 1 k λ have been plotted.

is 0.97 mJy (see above), we can conclude that the flux density of the radio halo on the NVSS amounts to ≈ 1.4 mJy.

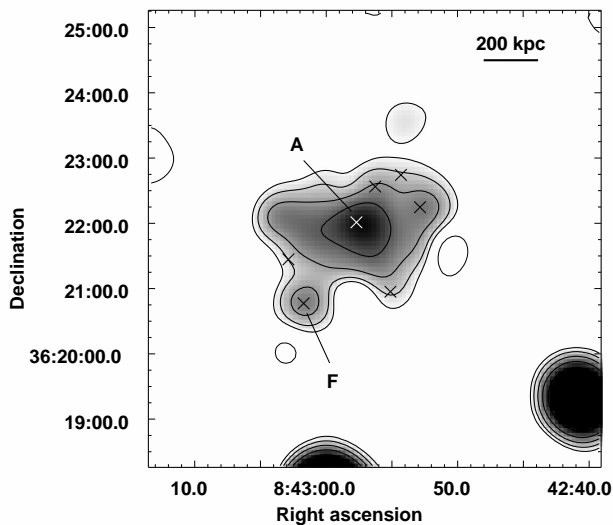


Fig. 4. Low resolution VLA-C 1.4 GHz image of the radio halo in A 697. The 1σ level in the image is $25 \mu\text{Jy b}^{-1}$. Contours are spaced by a factor 2 starting from $3\sigma = \pm 0.075 \text{ mJy b}^{-1}$. The restoring beam is $35.0'' \times 35.0''$, p.a. 0° . Crosses mark the position of the radio sources embedded in the halo emission.

3.2. Integrated radio spectrum

The observed integrated spectrum of radio halos may be affected by two main factors. In particular, (1) the contribution to the flux density of embedded individual radio sources, and (2) the u - v

coverage at short spacings.

Embedded individual sources are most likely of AGN origin, whose spectrum is flatter than radio halos. An inaccurate or inefficient subtraction of these sources may introduce a scatter of the flux density measurements at the various frequencies. On the other hand, the u - v coverage at short spacings may affect the detection of large scale structure.

We dealt with point (1) in Sect. 2.3 and 3.1. Point (2) will be the focus of Sect. 4.

All the available flux density measurements of the radio halo are reported in Table 4, along with the angular resolution of the images used for the measurements. The source is undetected on the Very Low-Frequency Sky Survey (VLSS), most likely due to the very poor sensitivity of the A 697 field.

The sources of uncertainty on the radio halo flux densities at 325 MHz and 1.4 GHz are the calibration errors and the procedure of point source subtraction, which we estimate sum up to $\sim 5\%$. The flux density value at 610 MHz is affected by a higher uncertainty. We performed an accurate check on flux density at 325 MHz, 610 MHz and 1.4 GHz for a number of discrete sources in the central field (see Fig. 1), using three images with the same angular resolution as the full resolution at 1.4 GHz ($\sim 16'' \times 16''$), after correction for the corresponding primary beam. We found that the 610 MHz measurements are systematically underestimated by $\sim 12\%$; after further inspection of the data, we concluded that this is due to an amplitude systematic error. Note that large residual calibration errors at 610 MHz were reported also for the cluster A 3562 in Giacintucci et al. (2005). Considering all this, the 610 MHz flux density value of the radio halo in A 697 given in VGD08 was corrected to account for this effect (Table 4 reports the new corrected value).

The integrated radio spectrum of the halo is shown in Fig. 6. The red solid line is the linear fit to the data (filled triangles) weighted for the uncertainties. A single power-law fit to the data gives a spectral index $\alpha = 1.8 \pm 0.1^4$

⁴ Giovannini et al. (2009) estimated a spectral index $\alpha_{325 \text{ MHz}}^{1.4 \text{ GHz}} = 1.2$ using our GMRT 325 MHz flux density value preliminary presented in Venturi et al. (2009) and the 1.4 GHz value derived from the original

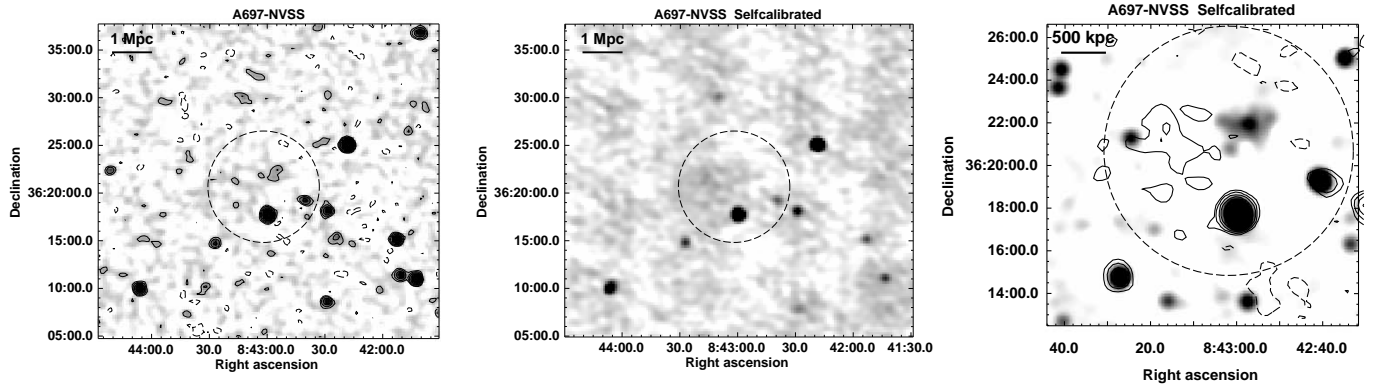


Fig. 5. *Left Panel:* Radio contours of the A 697 field from the public 1.4 GHz NVSS image (grey scale). The 1σ level is 0.45 mJy b^{-1} . Contour levels are spaced by a factor 2, starting from $\pm 1 \text{ mJy b}^{-1}$; the resolution is $45'' \times 45''$, p.a. 0° . *Central Panel:* 1.4 GHz image (grey scale) of the NVSS pointing containing A697 after new calibration. The 1σ level is 0.3 mJy b^{-1} . The resolution is $45'' \times 45''$. *Right Panel:* Recalibrated NVSS image (contours) overlaid on the VLA–C array 1.4 GHz image (same as Fig. 4). The first contour is $\pm 0.3 \text{ mJy b}^{-1}$, contours are spaced by a factor of 2. The dashed circle in each panel highlights the portion of the field referred to in Sect. 3.1.

Table 4. Flux densities of the radio halo in A 697.

ν (MHz)	S_ν (mJy)	HPBW "×"	Ref.
325	47.3 ± 2.7	46.8×41.4	this work; Fig. 2
610	14.6 ± 1.7	46.4×35.9	VGD08; see also this work Fig. 2
1400	3.7 ± 0.3	35.0×35.0	this work; Fig. 4*

* From VLA–C archival data (Obs. Id. AJ0252)

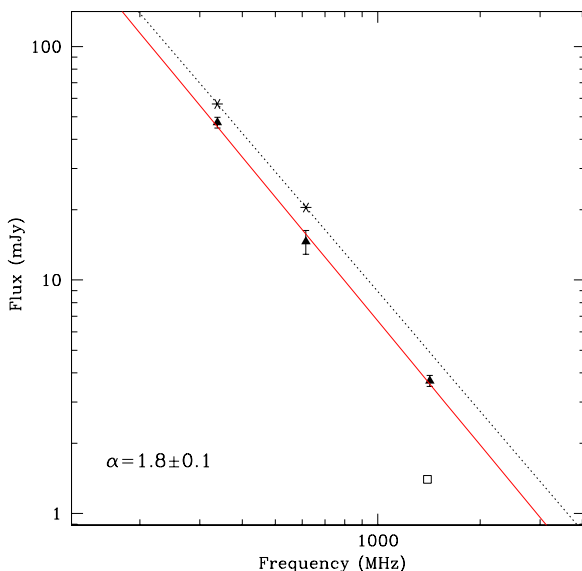


Fig. 6. Integrated radio spectrum of the halo. The red solid line is the linear fit to the data (filled triangles), weighted for uncertainties. The dashed line connects the two values of flux density including the estimated losses at 325 and 610 MHz (stars). The open square is the estimated flux density of the radio halo on the NVSS.

4. Uncertainties in the spectral slope

The combination of very low brightness emission and large angular size makes the imaging of faint radio halos a challenging process. The sampling of the $u-v$ coverage at short spacings is essential for a reliable imaging of extended and diffuse radio sources, and this is particularly relevant for faint radio halos, as is the case of A 697. The most serious effect of an inadequate $u-v$ coverage at short baselines is the loss of a fraction of the radio halo flux density, which may affect not only the imaging at an individual frequency, but also the integrated spectral index of the source. This effect becomes even more severe when only few data points over a small frequency range are available.

In this Section we will discuss the role of the $u-v$ coverage in the GMRT observations of A 697 and the implications on the spectral steepness of its giant radio halo. We will show that part of the total flux density of the radio halo could not be accounted for by the GMRT observations. This effect is more severe at 610 MHz, since Fig. 3 clearly shows that the inner portion of the $u-v$ coverage is much better sampled in the 325 MHz observations. Given that an underestimate of the 610 MHz flux density would reflect into a steeper spectrum, it is crucial that we test the reliability of the spectral index derived in the present work.

To constrain the spectral steepness of the radio halo, we estimated the flux density losses expected both in the 325 and 610 MHz GMRT data following the “fake” radio halos procedure, described in detail in VGD08. A “fake radio halo” is a model of the radio halo brightness profile, which consists of a set of optically thin concentric spheres with different radius and flux density. Here we briefly describe the main steps of this procedure and the results obtained.

4.1. The 325 MHz data

In order to evaluate the flux density loss on the halo at 325 MHz, families of fake radio halos were injected in the $u-v$ data. We chose different sets of values for the total flux density and largest

NVSS image. However, as shown in Sect. 3.1, the original NVSS value overestimates the flux density at the centre of A 697.

angular scale, and injected the fake halos in a region of the field free of point sources, and close enough to the cluster centre to avoid attenuation from the primary beam. We thus obtained a new dataset, which we will refer to as $(u-v)_{inj}$. The LAS of the injected fake radio halos (i.e. the diameter of the largest sphere of the model) ranges from $240''$ to $330''$, corresponding to a linear scale in the range $1 \div 1.4$ Mpc at the redshift of A 697. The total flux density values injected, S_{inj} , range from 50 to 70 mJy. We then imaged each new dataset $(u-v)_{inj}$ with the same parameters we used to produce the final low resolution image of the radio halo (see Fig. 2), and measured the flux density and LAS in each fake radio halo imaged. Note that both the fake and the real radio halos are imaged simultaneously, allowing a direct comparison between the two sources.

In general we found that the component with the largest angular size, i.e. the one with lowest surface brightness, is partially lost in the imaging process. On the contrary, the central highest surface brightness regions are well imaged. These general results are in agreement with what found in VGD08.

An injected fake halo with $S_{inj}=60$ mJy and $LAS=330''$ best reproduces the emission observed at the cluster centre, i.e. $S \simeq 48$ mJy and $LAS \simeq 300''$ (see Sect. 2.3). Based on these tests, we concluded that the expected flux density loss of the radio halo at 325 MHz is at most $\sim 20\%$. Most of this flux density is lost in the largest and lowest surface brightness component. The LAS of the real halo is $\sim 10\%$ smaller than that injected.

4.2. The 610 MHz data and the “revised” spectrum

Following the same procedure, we estimated the flux density loss at 610 MHz. A fake halo with $LAS=330''$ (same choice as for the injection at 325 MHz) and $S_{inj}=18$ mJy best reproduces the radio halo observed at 610 MHz. The resulting differential flux density loss between 325 MHz and 610 MHz is $\sim 20\%$. Based on these results, we estimated that the intrinsic flux density of the radio halo in A 697 is ~ 57 mJy at 325 MHz and ~ 20 mJy at 610 MHz (accounting for the 12% flux density correction derived in Sect. 3.2).

In Fig. 6 we report the integrated spectrum of the halo between 325 and 610 MHz taking into account the losses in flux density (the dashed line connects the two values, represented by the star symbols). The resulting spectral index is $\alpha_{rev} \sim 1.7$. We conclude that A 697 hosts a very steep spectrum radio halo. The flux density we measured at 1.4 GHz can be considered a lower limit, the upper one being the extrapolation of the “revised” spectrum between 325 MHz and 610 MHz. This leads to an “expected” flux density value $S_{1.4\text{ GHz}} \simeq 5$ mJy over the same region considered in this paper. Future high sensitivity observations at this frequency may allow us to constrain the high frequency end of the radio halo spectrum.

5. Discussion

We have presented observational evidence that A 697 hosts a very steep spectrum giant radio halo.

This source has observational properties similar to those of A 521, which we consider the prototypical example of ultra steep spectrum radio halos. In particular, it is barely detectable at 1.4 GHz with the current instruments, and with the observed values $\log P_{1.4\text{ GHz}}(\text{W/Hz}) = 23.95$ and $L_{X[0.1-2.4]\text{ keV}} = 1.06 \times 10^{45}$ erg s $^{-1}$, it lies below the well-known $\log P_{1.4\text{ GHz}} - \log L_X$ correlation for giant radio halos (see Brunetti et al. 2009 for a recent update). The source becomes stronger and considerably more

extended at lower frequencies. This is different from what is observed for those radio halos with spectral index $\alpha \sim 1.2 - 1.4$, whose overall morphology and size do not change appreciably moving down to lower frequencies (see for instance A 2744 and A 2219, Orrú et al. 2007; A 2319, Feretti et al. 2001; MACS J0717.5+3745, van Weeren et al. 2009 and Bonafede et al. 2009; RXCJ2003.5–2323, Giacintucci et al. 2009). Based on literature data, Giovannini et al. (2009) reported on four more halos with very steep integrated spectrum; however, the different resolutions and $u-v$ coverages, and the lack of accurate subtraction of individual embedded radio sources in heterogeneous datasets, may affect the shape and spectral index of the integrated spectra.

The observational connection between major cluster mergers and radio halos is a fairly well established result, both on the basis of individual studies (examples of recent multiband analysis may be found in Govoni et al. 2004; van Weeren et al. 2009; Bonafede et al. 2009; Giacintucci et al. 2009) and on statistical properties of large samples (see for instance Buote 2001 and VGB08). On the other hand, it has been recently suggested that the majority of radio halos should be generated during more common but less energetic mergers, for example between a massive cluster and a much smaller subcluster (with mass ratio $\gtrsim 5$) or between two similar clusters with mass $M \lesssim 10^{15} M_{\odot}$, which would trigger the formation of radio halos observable only up to few hundred MHz (Cassano et al. 2006 and Cassano 2009). So far, these elusive radio halos have been missed from large surveys mainly due to their steep spectrum, which requires very sensitive observations at frequencies $\nu \leq 1$ GHz. The discovery of the ultra steep spectrum radio halo in A 521 (Brunetti et al. 2008) provides observational support in favour of this idea.

The very steep spectrum radio halo found in A 697 offers a chance to further test the hypothesis of a connection between “low frequency radio halos” and less energetic cluster mergers.

5.1. The merger in the cluster A 697

Optical and X-ray observations are crucial tools to investigate cluster dynamics.

A detailed optical analysis of A 697 was carried out in G06, who found that the cluster is significantly far from dynamical relaxation. In particular, the observed complex dynamical state of A 697 might be explained either as an ongoing process of multiple accretion of small (≤ 0.2 Mpc) clumps by a very massive cluster, or as the result of a past merger event. The scenario may be even more complicated (major merger followed by multiple accretion), as suggested by the absence of a cool core in this cluster (Bauer et al. 2005). G06 concluded that it is difficult to provide more details on the type of merger in A 697, since most likely we are viewing the system at a small angle to the line of sight. Analysis of archival *Chandra* X-ray observations (G06) revealed the presence of significant substructure in the core region, with three clumps of emission within ~ 200 kpc from the centre, confirming the cluster complex dynamical state.

We re-analysed the public archive *Chandra* ACIS-I observation of A 697 (19.8 ks, OBSID 4271, presented also in G06). In Fig. 7 we report a newly wavelet-reconstructed *Chandra* image of A 697, with 325 MHz contours of the radio halo superposed (same image as right panel of Fig. 2). The X-ray image was obtained applying the wavelet decomposition tool (Vikhlinin, Forman & Jones 1997) to the cluster image in the 0.5–9 keV energy band, divided for the exposure map and background subtracted (see Giacintucci 2007 and references therein).

As clear from Fig. 7, the overall X-ray morphology of the cluster

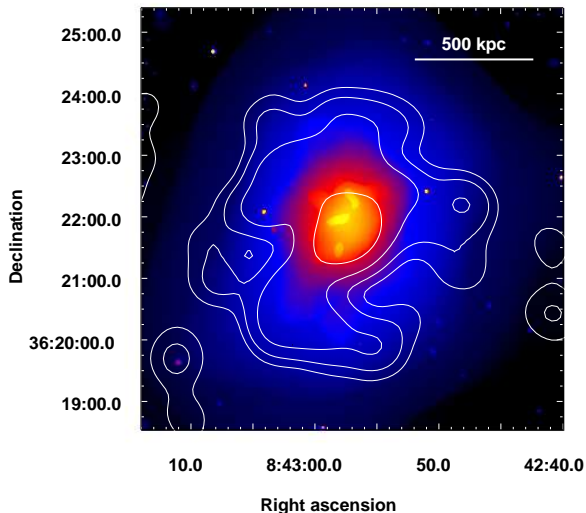


Fig. 7. Wavelet–reconstructed *Chandra* image of A 697, in the 0.5–9 keV band. The image is corrected for the exposure and background subtracted. Overlaid are the 325 MHz contours of the radio halo. The radio image is the same as right panel of Fig. 2.

is elliptical, and elongated along the North–North West/South–South East (NNW/SSE) direction. The extent and shape of the radio emission are in agreement both with the size of the X–ray emitting region and with the slight elongation along the NNW/SSE axis. Moreover, the peak of the radio emission covers the inner ~ 200 kpc of the core region, where the three X–ray subclumps are located. The cluster temperature and hardness ratio distributions were derived in Giacintucci (2007), with the calibration files available at the time. Gradients between the inner ~ 200 kpc core region and the surrounding areas were found both in the temperature and in the hardness ratio, in agreement with the proposed overall picture that A 697 is dynamically unrelaxed. Our analysis favours the multiple merger scenario, but unfortunately the short exposure time of the *Chandra* observations does not allow a more quantitative analysis.

5.2. Origin of the radio halo

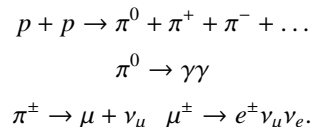
Theoretically, cosmic ray protons are expected to be the dominant non–thermal particle component in the ICM, due to their long life–time (see Blasi et al. 2007 for a recent review). However, current observations in different bands constrain the energy density of the non–thermal component to $< 10\%$ of the thermal gas in the central Mpc region of galaxy clusters (e.g. Brunetti et al. 2007; Churazov et al. 2008; Aharonian et al. 2009a and 2009b; Laganá et al. 2010).

As we mentioned in the introduction, it is presently believed that two main physical processes may contribute to the origin of the extended diffuse synchrotron emission in giant radio halos: the injection of secondary electrons through proton–proton collisions (hadronic models, e.g. Dennison 1980; Blasi & Colafrancesco 1999; Pfrommer & Ensslin 2004), and the in–situ re–acceleration of relativistic electrons by MHD turbulence generated in the ICM during cluster–cluster mergers (re–acceleration models, Brunetti et al. 2001, 2004; Petrosian 2001; Fujita et al. 2003; Cassano & Brunetti 2005).

Radio halos with very steep spectrum, i.e. $\alpha \geq 1.6$, are suitable targets to constrain these models and favour a turbulent re–acceleration scenario (Brunetti et al. 2008): in fact, in the context of the hadronic scenario, clusters hosting these radio halos must contain a very large population of cosmic ray protons. The observations presented in this paper suggest that Abell 697 hosts a very steep spectrum giant halo and this allows a prompt test of the hadronic model.

In this Section we assume that the giant radio halo in A 697 is of hadronic origin and discuss the consequences of this hypothesis on the physical properties of the ICM.

The decay chain that we consider for the injection of secondary particles in the ICM due to p–p collisions is (Blasi & Colafrancesco 1999):



that is a threshold reaction that requires protons with kinetic energy larger than $T_p \approx 300$ MeV.

Under the assumption that secondary electrons are not accelerated by other mechanisms, their spectrum approaches a stationary distribution due to the competition between injection and energy losses (Dolag & Ensslin 2000):

$$N_e^\pm(p) = \frac{1}{\left| \left(\frac{dp}{dt} \right)_{\text{loss}} \right|} \int_p^{p_{\text{max}}} Q_e^\pm(p) dp. \quad (1)$$

where Q_e^\pm is the injection rate of secondary electrons and radiative losses, that dominate for $\gamma > 10^3$ electrons in the ICM, are (Sarazin 1999) :

$$\left| \left(\frac{dp}{dt} \right)_{\text{loss}} \right| \simeq 3.3 \times 10^{-32} \left(\frac{p/m_e c}{300} \right)^2 \left[\left(\frac{B \mu G}{3.2} \right)^2 + (1+z)^4 \right]. \quad (2)$$

We follow standard formulae to calculate the injection rate of secondary electrons (Moskalenko & Strong 1998; Blasi & Colafrancesco 1999; Brunetti & Blasi 2005) and use Dermer’s fitting formulae for the inclusive p–p cross section (Dermer 1986) which allow to describe separately the rates of generation of π^- , π^+ and π^0 .

We assume a power law distribution of relativistic protons, $N_p(p) = K_p p^{-s}$, in which case the spectrum of secondaries at high energies, $\gamma > 10^3$, is $N_e(p) \propto p^{-(s+1)} \mathcal{F}(p)$, where \mathcal{F} accounts for the Log–scaling of the p–p cross section at high energies and makes the spectral shape slightly flatter than $p^{-(s+1)}$ (Brunetti & Blasi 2005; Brunetti 2009).

The synchrotron emissivity from secondary e^\pm is also obtained via standard formulae (Rybicki & Lightman 1979; see also Dolag & Ensslin 2000) :

$$\begin{aligned} J_{\text{syn}}(\nu) &= \sqrt{3} \frac{e^3}{m_e c^2} B \int_0^{\pi/2} d\theta \sin^2 \theta \int dp N_e(p) F\left(\frac{\nu}{\nu_c}\right) \\ &\propto n_{\text{th}} \epsilon_{\text{CR}} \frac{B^{1+\alpha}}{B^2 + B_{\text{cmb}}^2} \nu^{-\alpha} \end{aligned} \quad (3)$$

where

$$\epsilon_{\text{CR}} = K_p \int p^{-s} T_p dp \quad (4)$$

is the energy density of cosmic ray protons (T_p is the kinetic energy of protons), F is the synchrotron Kernel (Rybicki & Lightman 1979), ν_c is the critical frequency, and $\alpha \approx s/2 - \Delta$, $\Delta \sim 0.1 - 0.15$ due to the logarithmic scaling of the cross section (eg., Brunetti 2009). We adopt a value of the spectral index of the halo $\alpha = 1.75$ which is consistent with our observational findings and implies a spectral slope of the cosmic ray protons $s = 3.8$.

The diffuse emission of the radio halo is centered on the cluster core region and grossly resembles the X-ray morphology both in terms of extension and elongation (Fig. 7). The radio profile at 325 MHz, however is flatter than the X-ray profile, it drops by only a factor 5–6 at distance of 2.5–3 core radii (~ 500 kpc), suggesting a broad spatial distribution of the relativistic particles. Thus, we use a β -model for the spatial distribution of the cluster thermal gas (with parameters taken from Bonamente et al. 2006: $\beta=0.6$, $n_o = 9.8 \times 10^{-3} \text{cm}^{-3}$, $r_c = 42''$, i.e. ≈ 180 kpc, and gas temperature $kT = 10$ keV) and adopt a model (*Model 1*) of the distribution of relativistic components in Abell 697 where the energy density of both cosmic ray protons and magnetic field are *constant* with radius up to a distance $= 2.5 r_c$, and scale with that of the thermal gas at larger distances. This model gives a very good representation of the observed halo-radial profile up to a distance of about $2.5 r_c$ and, within the uncertainties, it is also in line with the observed profile at large distance (regardless of the strength of the magnetic field at $\leq 2.5 r_c$ distance).

In Fig. 8 we show the ratio of the energy density of non-thermal (relativistic protons and magnetic field) and thermal components in Abell 697 that is required assuming a hadronic origin of the radio halo. We find that for $B \leq 5 \mu\text{G}$ relativistic protons are required to store an energy comparable to (or larger than) that of the thermal ICM. The non-thermal energy content reaches a minimum for $B \approx 10 \mu\text{G}$, $\epsilon_{NT} \approx 1/3 \epsilon_{TH}$, implying an important dynamical contribution of the non-thermal components in the cluster. In addition, we point out that *Model 1* provides only a lower limit to the energy of the non-thermal components for two main reasons :

- 1) as soon as we include also the contribution from the tail of the proton energy distribution at sub-relativistic energies ($E < 1$ GeV), the required energy budget is much larger than that in Fig. 8 due to the steep proton spectrum, $\epsilon_{CR} \propto P_{min}^{-s+3}$.
- 2) the rather unphysical assumption in *Model 1* that the energy density of the non-thermal components is *constant* with radius (up $2.5 r_c$) yields a lower limit to the energy density of the cosmic ray protons that is required by the hadronic scenario. Indeed as soon as the magnetic field strength in Abell 697 is allowed to decrease with distance from the cluster centre, the energy density of relativistic protons must increase with radius and their total energy budget increases (Fig. 8).

We conclude that the very large energetics necessary for the non-thermal components assuming a hadronic origin of the halo disfavours this scenario.

6. Summary and conclusions

In this paper we presented 325 GMRT high sensitivity observations of the giant radio halo in A 697, and performed an accurate study of its integrated spectrum.

The largest extent of the radio halo at 325 MHz is $\sim 5'$ (corresponding to $1.3 \text{ Mpc } h_{70}^{-1}$), and it is considerably larger than at higher frequencies. The radio spectrum, determined with three

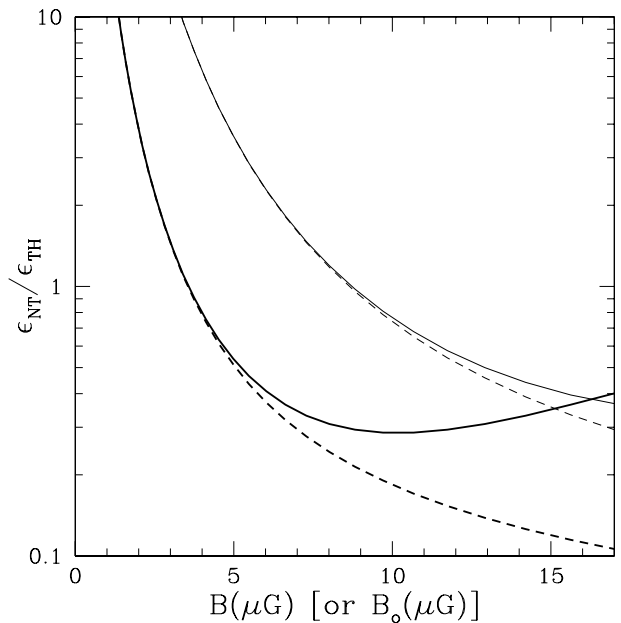


Fig. 8. The ratios between the energy densities of relativistic protons and thermal ICM (dashed lines) and between non-thermal (relativistic protons and magnetic field) and thermal ICM (solid lines) are shown as a function of magnetic field. All energy densities are calculated within a distance $r \sim 3 r_c$, i.e. roughly the region filled by the radio halo. Thick lines refer to *Model 1*, in which case B is that within $2.5 r_c$. Thin lines are obtained by assuming that the magnetic field energy-density scales with the thermal one, $B = B_o (n_{th}/n_o)^{1/2}$ (e.g. Govoni & Feretti 2004; with thermal quantities taken from Bonamente et al. 2006), and by leaving the radial profile of relativistic protons free to vary with distance (up to $r \sim 2.5 r_c$ while at larger distances it is assumed to scale with thermal one as in *Model 1*) in order to match the observed synchrotron profile; in this latter case the x-axis shows the central field value, B_o .

data points in the frequency range 325 MHz–1.4 GHz, has a spectral index $\alpha_{325 \text{ MHz}}^{1.4 \text{ GHz}} = 1.8 \pm 0.1$. An accurate analysis of the fraction of flux density that might be missed in our observations due to the u-v coverage at short spacings led to an estimated spectral index $\alpha_{rev}=1.7$. We thus conclude that A 697 hosts a very steep spectrum radio halo.

A qualitative analysis of the X-ray emission from the ICM suggests that this cluster is unrelaxed. Comparison with the 325 MHz emission from the radio halo shows that the non-thermal and thermal emissions have a similar morphology. Though at a qualitative level, the observations are in agreement with the idea that A 697 is the result of a multiple merger.

Similarly to the case of A 521, we showed that the very steep spectrum of the halo disfavours a hadronic origin, which would require an unphysically large energy budget. On the other hand, models based on turbulent acceleration for the origin of radio halos predict a large number of halos in the Universe with very steep spectrum. This can be tested as soon as LOFAR and LWA will become operational.

Acknowledgements. We thank the staff of the GMRT for their help during the observations. GMRT is run by the National Centre for Radio Astrophysics of the Tata Institute of Fundamental Research. This research is partially funded by INAF and ASI through grants PRIN-INAF 2007, PRIN-INAF 2008 and ASI-INAF I/088/06/0. This research has made use of the NASA/IPAC Extragalactic Database (NED) which is operated by the Jet Propulsion Laboratory, California

Institute of Technology, under contract with the National Aeronautics and Space Administration.

References

- Abell, G.O., Corwin, H.G.Jr., & Olowin, R.P., 1989, ApJS, 70, 1
- Aharonian, F., Akhperjanian, A.G., Anton, G., et al., 2009a, A&A, 495, 27
- Aharonian, F., Akhperjanian, A.G., Anton, G., et al., 2009b, A&A, 502, 437
- Bauer, F.E., Fabian, A.C., Sanders, J.S., et al., 2005, MNRAS, 359, 1481
- Bacchi, M., Feretti, L., Giovannini, G., et al., 2003, A&A, 400, 465
- Blasi, P., & Colafrancesco, S., 1999, APh 12, 169
- Blasi, P., Gabici, S., & Brunetti, G., 2007, Int. Journal of Modern Physics A, 22, 681
- Bonafede, A., Feretti, L., Giovannini, G., et al., 2009, A&A, 503, 707
- Bonamente, M., Joy, M. K., LaRoque, S. J., et al., 2006, ApJ, 647, 25
- Brunetti, G., Setti, G., Feretti, L., et al., 2001, MNRAS, 320, 365
- Brunetti, G., 2004, JKAS, 37, 493
- Brunetti, G., & Blasi, P., 2005, MNRAS, 363, 1173
- Brunetti, G., Venturi, T., Dallacasa, D., et al., 2007, ApJ, 670L, 5
- Brunetti, G., Giacintucci, S., Cassano, R., et al., 2008, Nature, 455, 944
- Brunetti, G. 2008, astro-ph/0810.0692
- Brunetti, G., 2009, A&A, 508, 599
- Brunetti, G., Cassano, R., Dolag, K., et al., 2009, A&A, 507, 661
- Buote, D. A., 2001, ApJ, 553, L15
- Cassano, R., & Brunetti, G., 2005, MNRAS, 357, 1313
- Cassano, R., Brunetti, G., & Setti, G., 2006, MNRAS 369, 1577
- Cassano, R., 2009, in *The Low Frequency Radio Universe*, Eds. D.J. Saikia, D.A. Green, Y. Gupta & T. Venturi, ASP Conf. Ser. 407, 223
- Churazov, E., Forman, W., Vikhlinin, A., 2008, MNRAS, 388, 1062
- Condon, J. J., Cotton, W. D., Greisen, et al., 1998, The Astronomical Journal, Volume 115, Issue 5, pp. 1693-1716
- Dahle, H., Kaiser, N., Irgens, R.J., et al., 2002, ApJS, 139, 313
- Dallacasa, D., Brunetti, G., Giacintucci, S., et al. 2009, ApJ, 699, 1288
- De Filippis, E., Sereno, M., Bautz M.W., et al., 2005, ApJ, 625, 108
- Dennison, B., 1980, ApJ, 239, L93
- Dermer, C.D., 1986, A&A, 157, 223
- Dolag, K., Ensslin, T.A., A&A, 362, 151
- Ebeling, H., Edge, A.C., Bohringer, H., et al., 1998, MNRAS, 301, 881
- Feretti, L., Fusco-Femiano, R., Giovannini, G., et al. 2001, A&A, 373, 106
- Ferrari, C., Govoni, F., Schindler, S., et al., 2008, Space Science Reviews, Vol. 134, p. 93
- Fujita, Y., Takizawa, M., Sarazin, C.L., 2003, ApJ, 584, 190
- Giacintucci, S., Venturi, T., Brunetti, G., et al., 2005, A&A, 440, 867
- Giacintucci S., PhD Thesis *Multiwavelength study of cluster mergers and consequences for the radio emission properties of galaxy clusters*, University of Bologna; <http://amsdottorato.cib.unibo.it/353/>
- Giacintucci, S., Venturi, T., Brunetti, G. et al., 2009, A&A, 505, 45
- Giovannini, G., Tordi, M., & Feretti, L., 1999, New Astron., 4, 141
- Giovannini, G., Bonafede, A., Feretti, L., et al., 2009, A&A, 507, 1257
- Girardi, M., Boschini, W., & Barrena, R., 2006, A&A, 455, 45 (G06)
- Govoni, F., Feretti, L., Giovannini, G., et al., 2001, A&A, 376, 803
- Govoni, F., Markevitch, M., Vikhlinin, A., et al., 2004, ApJ, 605, 695
- Govoni, F., & Feretti, G., 2004, International Journal of Mod. Phys. D., V. 13, 8, 1549
- Jaffe, W.J., 1977, ApJ, 212, 1
- Kempner, J.C., & Sarazin, C.L., 2001, ApJ, 548, 639
- Laganá, T.F., de Souza, R.S., & Keller, G.R., 2010, A&A, 510, 76
- Metzger, M.R., & Ma, C.P., 2000, AJ, 120, 2879
- Moskalenko, I.V., & Strong, A.W., 1998, ApJ, 493, 694
- Orrú, E., Murgia, M., Feretti, L., et al., 2007, A&A, 467, 943
- Ota, N., & Mitsuda, K., 2004, A&A, 428, 757
- Petrosian, V., 2001, ApJ, 557, 560
- Frommer, C., Enßlin, T.A., 2004, JKAS, 37, 455
- Rengelink, R.B., Tang, Y., de Bruyn, A.G., et al., 1997, A & A Supplement series, Vol. 124, August 1997, 259-280
- Rybichi, G.B., & Lightman, A.P. 1979, Astronomy Quarterly, V. 3, 199, 1980
- Sarazin, C.L., 1999, ApJ, 520, 529
- van Weeren, R.J., Rotgering, H.J.A., Brügger, M., et al., 2009, A&A, 505, 991
- Venturi, T., Giacintucci, S., Brunetti, G., et al., 2007, A&A, 463, 937 (VGB07)
- Venturi, T., Giacintucci, S., Dallacasa, D., et al., 2008, A&A, 484, 327 (VGD08)
- Venturi, T., Giacintucci, S., Cassano, R., et al., 2009, in *The low frequency Universe*, Eds. D.J. Saikia, D.A. Green, Y. Gupta & T. Venturi, ASPC 407, 232
- Vikhlinin, A., Forman, W., & Jones C., 1997, ApJ, 474, L7